ELSEVIER

Polymer 42 (2001) 7765–7780

polymer

www.elsevier.nl/locate/polymer

# Gas sorption and transport in poly(alkyl (meth)acrylate)s. I. Permeation properties

Z. Mogri, D.R. Paul*

*Department of Chemical Engineering and Texas Materials Institute, The University of Texas at Austin, Austin, TX 78712, USA*

Received 12 December 2000; received in revised form 30 March 2001; accepted 2 April 2001

**Abstract**

The gas permeability of poly(alkyl acrylate)s was measured as a function of temperature in both the amorphous and crystalline states. Penetrant permeability in the amorphous state increases as the side-chain length becomes longer but shows mixed trends in the crystalline state. A decrease in permeability was observed in the amorphous state when the backbone was stiffened, i.e. polymethacrylate versus polyacrylate. The influence of side-chain length and backbone stiffness on the magnitude of the change in permeability upon traversing the melting point, or permeability switch, is discussed. The effect of main versus side-chain crystallinity on the permeation switch is analyzed. The influence of a compositional change in the amorphous phase upon melting on the gas permeability of side-chain crystalline polymers is addressed. 

*Keywords*: Side-chain crystalline polymers; Alkyl acrylates; Permeation switch

## 1. Introduction

The physical structure and thermal properties of poly(alkyl acrylate)s, poly(alkyl methacrylate)s, and other polymer backbones with pendant alkyl chains have been extensively investigated [1–15]. These side-chain crystalline polymers find use in applications involving agriculture, medicine, and food packaging [16,17]. This utility stems from the striking difference in several polymer properties upon traversing the melting point, including permeability to small molecules; however, the fundamental mechanisms of penetrant transport in side-chain crystalline polymers have not been extensively explored [18].

On the other hand, the gas transport properties of main-chain crystalline polymers have been extensively investigated, especially polyethylene [19–28]. Gas transport in these systems is usually discussed in terms of the two-phase model, which views crystallites as an impermeable phase with all diffusion occurring in the amorphous phase [19–21]. The degree of crystallinity, crystallite size, shape, and orientation (overall morphology), all of which depend on thermal history, influence gas transport properties. There is evidence that the crystallites tend to impede penetrant mobility in the surrounding amorphous phase.

Previous work from this laboratory documented gas sorption and transport properties of poly(octadecyl acrylate) in the semi-crystalline and molten states [18]. A dramatic change in permeability was observed as the melting point was traversed. The permeability jump on melting was found to be penetrant dependent, which was qualitatively attributed to chain immobilization in the amorphous phase caused by the presence of crystallinity. Solubility measurements above and below the melting point are not in full agreement with the expectation of the simple two-phase model that solubility properties of the amorphous phase are not affected by the crystallites [21].

The simple two-phase model was developed for polymers with main-chain crystallinity where the amorphous and crystalline phases have the same chemical structure. The situation for side-chain crystallinity is more complex since the crystals are comprised of alkyl material only while the amorphous phase contains the backbone plus some residual portions of the alkyl side-chain. Thus, the amorphous phase changes chemical composition upon melting. One objective of this paper is to further explore differences between the permeation jump on melting of main- and side-chain crystalline polymers and to assess the contribution from compositional change for the latter. How side-chain length affects the semi-crystalline state permeability and consequently, the permeation jump, will also be explored. The effect of backbone stiffness on these same properties will be discussed.

* Corresponding author. Tel.: +1-512-471-5392; fax: +1-512-471-0542.
*E-mail address:* drp@che.utexas.edu (D.R. Paul).

0032-3861/01/$ - see front matter 
PII: S0032-3861(01)00260-9

## 2. Background

### 2.1. Thermal and structural properties of poly(n-alkyl (meth)acrylate)s

The dependence of side-chain length on the thermal and structural properties of poly(alkyl acrylate)s and poly(alkyl methacrylate)s has been explored [1,2,5]. Jordan et al. observed side-chain crystallinity at a critical number of carbons for the poly(alkyl acrylate) series. From DSC measurements, this crystallinity develops independent of the backbone for side-chains containing approximately 10 carbon atoms or more. Due to higher backbone stiffness, the methacrylate polymers have lower melting points and lower degrees of crystallinity [5]. This reduction in flexibility reduces conformational freedom of the side-chain, resulting in less favorable packing [5,11,12].

It is generally argued that a two-layer structure predominates for the poly(alkyl acrylate)s while, due to backbone stiffness, a one-layer structure has been proposed for the poly(alkyl methacrylate)s. The two layer structure views the side-chains packing end-to-end, perpendicular to the backbone. Some researchers advocate that the one-layer structure is of similar form [5] (with a different characteristic d-spacing) but others argue for interdigitating side-chains [10,13,14,29,30]. However, depending on the crystallization conditions, one-layer and mixed structures have also been reported [5,30]. The temperature dependence of this characteristic layer d-spacing has also been studied. The molten layer structure was proposed as a single layer for poly(alkyl (meth)acrylate)s [5].

### 2.2. Effect of side-chain length and backbone stiffness on permeability

The effect of polymer structure on gas transport properties has been extensively reported in the literature and the subject of several reviews [31–34]. A few studies have focused on the effect of pendant group chain length on gas transport properties [35–44]. As the side-chain becomes longer, the penetrant permeability may increase, decrease, or not change depending on the polymer backbone structure and free volume.

Masuda et al. reported no change in gas permeability for the poly(1-(*n*-alkylthio)-1-propyne) series up to 10 methylene units in the alkyl side-chain [37]. Decreases in permeability were observed for the poly(silyl propyne)s with increasing side-chain length [38,39]. Morisato et al. reported increasing permeability with increasing side-chain length for the –(RC═CR′)– series, where R = $CH_3$ and R′ is the alkyl side-chain [35]. However, when R = Cl, the permeability decreases then increases on going from R′═$C_4H_9$ to $C_6H_{13}$ then to $C_8H_{17}$ [36]. Similar side-chain length dependence is also found in polynorbornenes (prepared by addition polymerization) containing an alkyl side-chain pendant group [43]. The permeability decreases as the alkyl goes from methyl to hexyl but begins to increase at the decyl side-chain [43]. Interestingly, a series of siloxanyl substituted polynorbornenes (prepared by ring opening polymerization) starting with an ethyl substituent and proceeding to propyl and butyl showed increasing permeabilities in that order [44]. Lower $T_g$ polymers than those described above show the permeability to increase as the side-chain is lengthened, e.g. poly(alkyl phosphazene)s [42], amorphous polyamides (extension of the polymer backbone) [40], poly(*N*-*n*-alkyl maleimide)s [45,46], and poly(alkyl sulfone)s [41] display this behavior. Clearly, chain rigidity, in relation to the glass transition temperature, and free volume play a large part in the interpretation of the above findings.

The polymers investigated here have a rubbery amorphous phase at the temperatures studied [9,18,47,48], and based on the trends indicated above, we expect that increasing the side-chain length will lead to higher permeability in the completely amorphous state. For a given side-chain length, we expect a methacrylate polymer to have a lower permeability than an acrylate polymer in the completely amorphous state. One might expect the permeability to asymptote at the value of molten polyethylene as the side-chain becomes very long; this issue will be addressed in a later section.

### 2.3. Gas transport mechanisms in semi-crystalline rubbery polymers

Gas transport through rubbery polymers proceeds through a solution-diffusion mechanism

$$P = DS, \tag{1}$$

where the Henry's law solubility coefficient of the gas, $S$, represents thermodynamic factors, while the diffusion coefficient, $D$, reflects kinetic factors. Both the solubility and diffusion coefficients must be modified to account for the presence of crystallites in the polymer, which is usually described within the framework of a two-phase model proposed by Michaels and Bixler for PE [19–21]. The proposed equations are

$$S = S^*\alpha \tag{2}$$

$$D = D^*/\tau\beta \tag{3}$$

where $S^*$ and $D^*$ are the solubility and diffusivity of the completely amorphous polymer, $\alpha$ the amorphous volume fraction, $\tau$ the tortuosity, and $\beta$ is a chain immobilization factor. These models, their significance, and validity have been analyzed in a previous publication [18]. The temperature dependence of the transport parameters follows Arrhenius type expressions for both the semi-crystalline and molten states.

A prior paper quantitatively characterized the permeability switch or jump resulting from the melting of the crystallites [18] in terms of the ratio $P_T^+/P_T^-$, where $P_T^-$ is

the permeability of the semi-crystalline state (−) extrapolated to temperature $T$ and $P_T^+$ is the extrapolation from the molten state (+) to this same temperature. We arbitrarily set $T = T_m$. The permeation switch ratio $P_T^+/P_T^-$ is equal to $\tau\beta/\alpha$ in terms of the model represented by Eqs. (1)–(3) [18].

Side-chain crystalline poly(octadecyl acrylate) or PA-18 was previously shown to have a permeation switch ratio ranging from approximately 10 to 100 depending on the penetrant. This penetrant dependent permeation switch cannot be explained simply by the elimination of the tortuous path around impenetrable crystallites. Main-chain crystalline polymers, such as polyethylene, at similar levels of crystallinity, have significantly lower switch ratios, which are less dependent on the size of the penetrant. The PA-18 permeation jump was found to be predominantly diffusion based, and the penetrant size effect was attributed to chain immobilization, accounted for by the factor $\beta$. Differences in crystalline morphology and extent of chain immobilization are believed to be responsible for the higher magnitude of the permeation jump observed for side-chain crystalline materials [18].

According to the simple model embodied in Eqs. (1)–(3), the solubility part of the permeability switch ratio, i.e. $S_T^-/S_T^+$, should equal the amorphous fraction $\alpha$; however, the experimental solubility ratio is not equal to the value of $\alpha$ determined by DSC. This may be attributed, at least in part, to the change in composition on melting mentioned earlier that is not accounted for in the Michaels and Bixler model; there is no change in composition on melting the main-chain crystalline polymers. Gas permeability coefficients in the amorphous phase will be shown to depend strongly on the length of the alkyl side-chain and this accounts for part of the magnitude of the permeation jump. The dependence of the solubility and diffusion coefficients on the amorphous phase composition will be described in the second part of this series.

## 3. Materials and methods

Methyl and ethyl acrylate monomers and polycaprolactone (PCL) were purchased from Aldrich Chemical Company while decyl acrylate monomer was purchased from Polysciences. Monomers of tetradecyl, octadecyl, and behenyl acrylate and octadecyl methacrylate were generously donated by Landec Corporation. Solution polymerizations were done in toluene or heptane at 60°C for times ranging from 2 h for methyl and ethyl acrylate to 24 h for side-chains of length decyl and above. Monomer and polymer purification and initiator concentrations were described previously [18].

Poly(2,6-dimethyl-1,4-phenylene oxide) (PPO), generously provided by GE Plastics (intrinsic viscosity = 0.46 dl/g, $M_w = 46,000$), was used to coat Anopore™ (Whatman) porous ceramic discs (pore diameter = 0.02 $\mu$m) which were used without the annular polypropylene support ring. The choice of the support, the PPO modification, membrane formation techniques, permeation protocol, and data analysis were described previously [18,48].

The methyl and ethyl acrylate polymers (PA-1 and PA-2) were cast onto Teflon plates from a tetrahydrofuran solution containing 5–10 wt% polymer. These films were allowed to dry for approximately three days then placed in a vacuum oven at 100°C for one day. The films were removed from the plates using liquid nitrogen. A section of these films was placed on the PPO coated support for permeation measurements. PA-1 did not adhere well to the PPO layer; thus, it was necessary to mask the permeation area on the upstream as well as the downstream surfaces. Note that this is the only polymer for which the membrane formation technique reported earlier [48] had to be modified.

Decyl and tetradecyl acrylate polymers (PA-10 and PA-14) were directly cast on the PPO modified supports, without solvent, in a vacuum oven at elevated temperatures. The polymer was sufficiently fluid to form a uniform film after approximately one day in this environment. Octadecyl and behenyl acrylate polymers (PA-18 and PA-22) and poly(octadecyl methacrylate) (PMA-18) were cast onto glass plates from a toluene solution containing 10 wt% polymer. A similar procedure was used for PCL with chloroform as the solvent. These films were allowed to dry for approximately two days in a fume hood then placed in a vacuum oven at room temperature for 24 h before use. A portion of the films was then placed on the PPO modified support for permeation measurements.

The equipment and techniques for measurement of density, film thickness, melting point, heat of fusion, molecular weight, and permeability were described previously [18,48].

## 4. Results and discussion

The physical and thermal properties of the polymers investigated here are described followed by presentation of their permeability to various gases as a function of temperature. The effect of side-chain length on gas transport properties of the alkyl acrylate polymers in the completely amorphous state and below the melting point are discussed next; the trends for the latter are more complex owing to the physical effects of crystalline texture superimposed on top of the effect of repeat unit structure observed above the melting point. The permeability properties of PCL in the amorphous and crystalline states are addressed in the next section. A comparison of the switch effect for main- and side-chain crystalline polymers along with an analysis of the effect of composition change on melting are made in the last sub-section.

### 4.1. Physical and thermal properties

The density and molecular weight of the polymers

Table 1
Physical properties of the polymers studied in this work

| Polymer | Acronym | Experimental density (g/cm$^3$) | Estimated density (g/cm$^3$)[a] | $M_w$ |
|---|---|---|---|---|
| Poly(methyl acrylate) | PA-1 | 1.221 | 1.237 | 225,000 |
| Poly(ethyl acrylate) | PA-2 | 1.1178 | 1.164 | 1,300,000 |
| Poly(decyl acrylate) | PA-10 | – | 0.986 | 149,000 |
| Poly(tetradecyl acrylate) | PA-14 | – | 0.980 | 209,000 |
| Poly(octadecyl acrylate) | PA-18 | 0.9754 | 0.976 | 551,000 |
| Poly(behenyl acrylate) | PA-22 | 0.9752 | 0.973 | 119,000 |
| Poly(octadecyl methacrylate) | PMA-18 | 0.9672 | 0.970 | 210,000 |
| Polycaprolactone | PCL | – | – | 65,000 |

[a] From Ref. [49].

investigated are shown in Table 1. For polymers that were fluid at room temperature, the density was estimated by a group contribution method [49] since the density gradient column technique could not be used. The molecular weights were sufficient to form useful films.

Values of the melting point ($T_m$) and heat of fusion ($\Delta H_f$) measured by DSC are shown in Table 2 as a function of the thermal history of the polymer. The degree of crystallinity ($x_c$) was calculated from

$$x_c = \frac{\Delta H_f}{\Delta H_{fo}}, \tag{4}$$

where the value of $\Delta H_{fo}$ is 52.5 cal/g crystal for alkyl side-chain polymers [1,5] and 35.5 cal/g crystal for PCL [49]. The values of $T_m$ and $\Delta H_f$ generally agree with those reported in the literature, though thermal history was not specified in these investigations [1,5].

### 4.2. Gas permeability versus temperature

The permeability coefficients of PA-14, PA-22, PMA-18, and PCL in the semi-crystalline and molten state for various gases are presented in Figs. 1–4. The semi-crystalline state was developed in a controlled manner by cooling from the melt at either 0.1 or 1.0°C/min. The permeability coefficient follows an Arrhenius temperature dependence, except in the immediate vicinity of the polymer $T_m$. Just below $T_m$, the permeability begins to increase rapidly as the crystals melt, eventually an Arrhenius dependence (with a different activation energy) is again established above the $T_m$. This is illustrated in Fig. 1 for poly(tetradecyl acrylate) or PA-14, where data are shown over the melting range; subsequent figures do not show data in the melting region.

Table 2
Thermal properties of the polymers studied in this work

| Polymer | Thermal history[a] (°C/min) | $T_m$ (°C) | $\Delta H_f$ (cal/g) | $x_c$ |
|---|---|---|---|---|
| PA-14 | 0.1 | 28 | 12.8 | 0.24 |
| PA-18 | 1.0 | 50 | 19.3 | 0.37 |
| PA-18 | 0.1 | 52 | 21.6 | 0.41 |
| PA-22 | 1.0 | 70 | 24.6 | 0.47 |
| PA-22 | 0.1 | 72 | 26.4 | 0.50 |
| PMA-18 | 0.1 | 39 | 12.7 | 0.24 |
| PCL | 1.0 | 56 | 14.9 | 0.42 |

### 4.3. Gas permeability of amorphous poly(alkyl acrylate)s

The gas permeability of amorphous poly(alkyl acrylate)s is presented graphically in Fig. 5 as a function of the length of the alkyl side-chain, also see Table 3. These data were measured at, or extrapolated from above $T_m$ to, 35°C. The error in extrapolating such data in the amorphous state is no more than 10% judged by the reproducibility of the data. Within experimental error, the trend is for the permeability of each gas to increase as the side-chain is lengthened. An increase in free volume as additional methylenes are added in the amorphous state is the likely reason for the increase in permeability. This trend has its primary basis in diffusion

Table 3
Comparison of gas permeability coefficients ($P$) and activation energies for gas permeation ($E_p$) for molten or rubbery state poly(alkyl acrylate)s and PCL

| Polymer | | He | $H_2$ | $O_2$ | $N_2$ | $CH_4$ | $CO_2$ |
|---|---|---|---|---|---|---|---|
| PA-1 | $P$[a] | 12.4 | 10.6 | 1.06 | 0.24 | 0.29 | 9.58 |
| | $E_p$[b] | 7.3 | 9.3 | 12.5 | 14.5 | 17.2 | 12.7 |
| PA-2 | $P$ | 44.0 | 60.4 | 19.0 | 6.46 | 14.9 | 176 |
| | $E_p$ | 5.5 | 5.8 | 7.1 | 8.4 | 8.1 | 5.0 |
| PA-3[c] | $P$ | 46.3 | 61.6 | 24.3 | 7.85 | 19.7 | 182 |
| PA-10 | $P$ | 57.0 | 92.7 | 47.6 | 19.0 | 47.8 | 261 |
| | $E_p$ | 5.3 | 5.5 | 5.8 | 6.9 | 6.8 | 4.2 |
| PA-14 | $P$ | 52.9 | 96.2 | 57.1 | 22.1 | 65.1 | 297 |
| | $E_p$ | 5.7 | 5.7 | 5.7 | 6.6 | 6.5 | 3.8 |
| PA-18 | $P$ | 68.8 | 113 | 75.0 | 29.1 | 90.8 | 428 |
| | $E_p$ | 5.4 | 6.3 | 5.2 | 6.3 | 5.6 | 2.7 |
| PA-22 | $P$ | 73.5 | 146 | 76.3 | 36.0 | 93.4 | 404 |
| | $E_p$ | 4.9 | 4.4 | 4.6 | 4.8 | 4.9 | 2.9 |
| PCL | $P$ | 29.3 | 52.4 | 25.3 | 9.51 | 22.6 | 288 |
| | $E_p$ | 5.6 | 5.2 | 5.0 | 5.7 | 5.8 | 1.9 |

[a] $P$ measured at or extrapolated to 35°C and has units of Barrers.
[b] $E_p$ has units of kcal/mol.
[c] Calculated from best fit lines of Fig. 5.

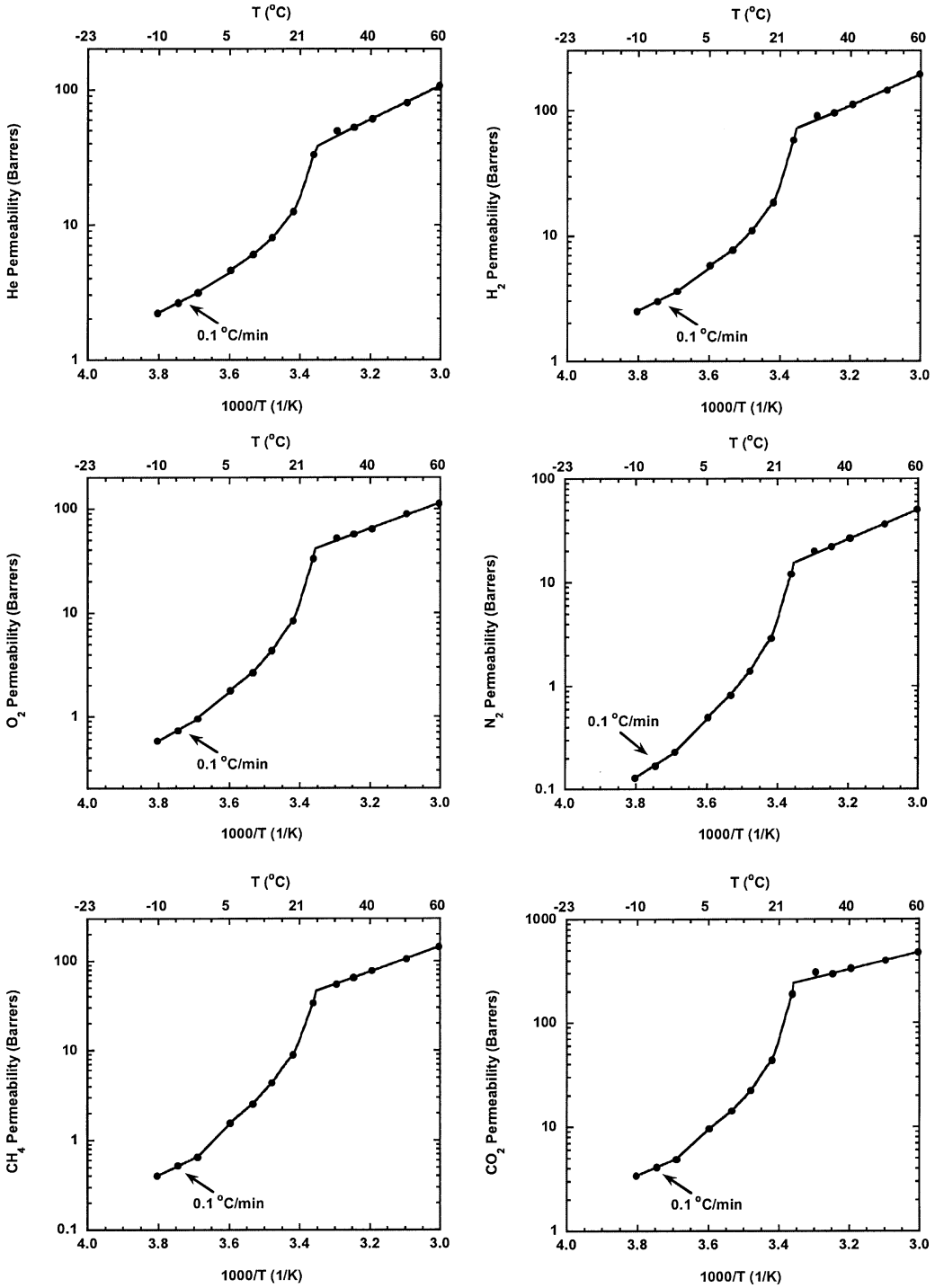


Fig. 1. He, $H_2$, $O_2$, $N_2$, $CH_4$, and $CO_2$ permeability (Barrers) of poly(tetradecyl acrylate) (PA-14) as a function of temperature.

not solubility, which will be discussed in the second part of this series. The activation energy of permeation generally decreases as side-chain length increases, see Table 3, which is consistent with the permeability increase.

As seen in Fig. 5, for each gas there is a steep increase in permeability from PA-1 to PA-2; the extent of the increase is strongly penetrant dependent. There is a more gradual and fairly linear increase in permeability with additional methylenes. The arithmetic scale of this figure is a useful way to represent this trend. However, in this presentation the permeability of many penetrants appear to be essentially zero for PA-1. It is instructive to view the data using a logarithmic permeability scale as shown in Fig. 6 for $CH_4$ and $CO_2$. This representation shows even more dramatically the large increase in permeability as the alkyl goes from methyl to ethyl.

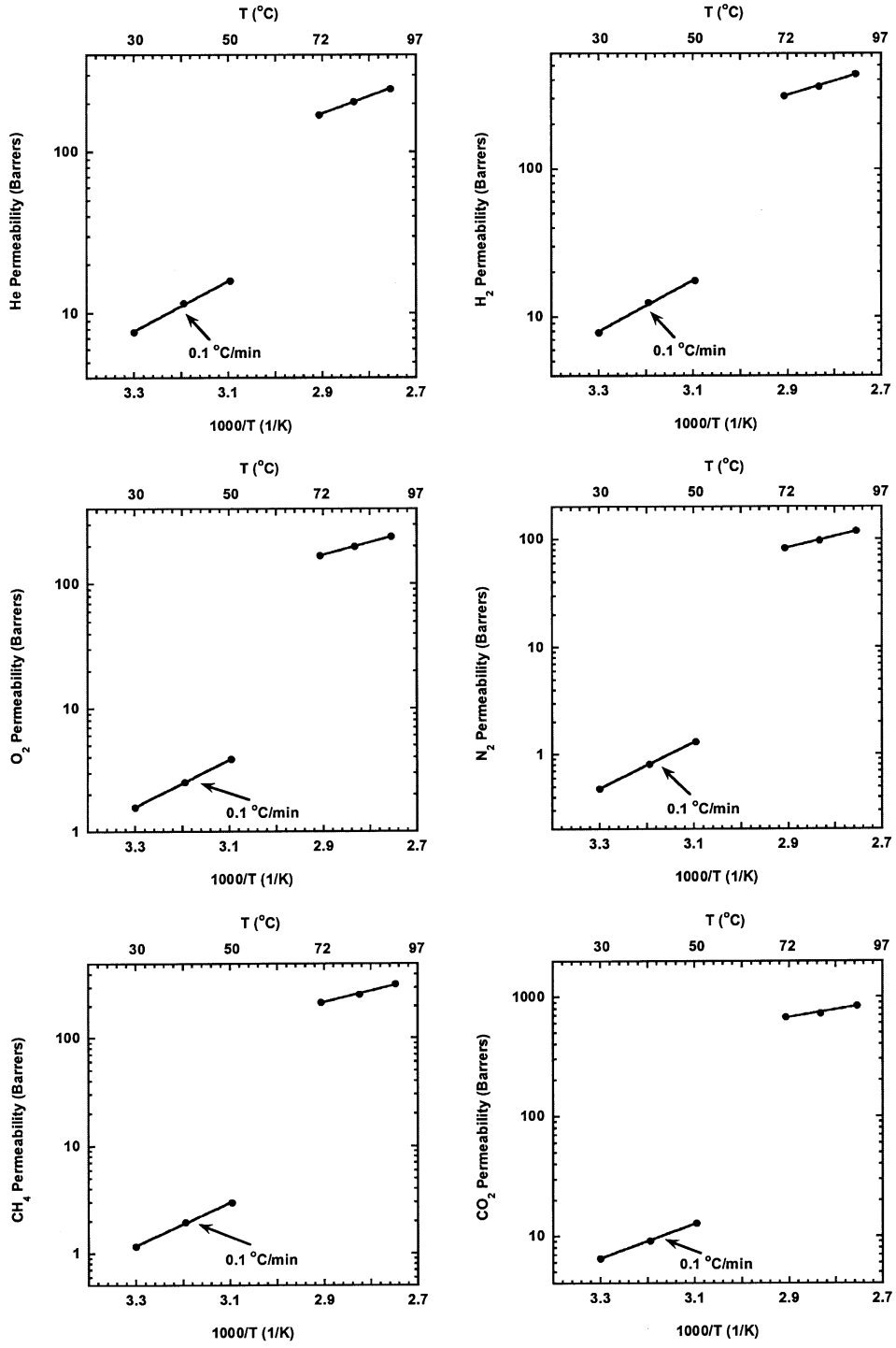


Fig. 2. He, $H_2$, $O_2$, $N_2$, $CH_4$, and $CO_2$ permeability (Barrers) of poly(behenyl acrylate) (PA-22) as a function of temperature.

Because of the dramatic differences between PA-1 and PA-2, we felt it was necessary to examine PA-1 more carefully to ensure that these permeability coefficients are indeed accurate. Poly(methyl acrylate) (PA-1) was previously studied in our laboratory [50] using a low density polyethylene film to prevent this rubbery polymer from penetrating the porous support material during measurement. The effect of the polyethylene was subtracted using the series resistance model. The values presented here are higher by 17% for He to 33% for $CO_2$ compared to these previous results. The selectivities are quite similar. A membrane formation technique that utilized an upstream surface mask was common to both studies. The permeability values were reproducible in this study at different temperatures

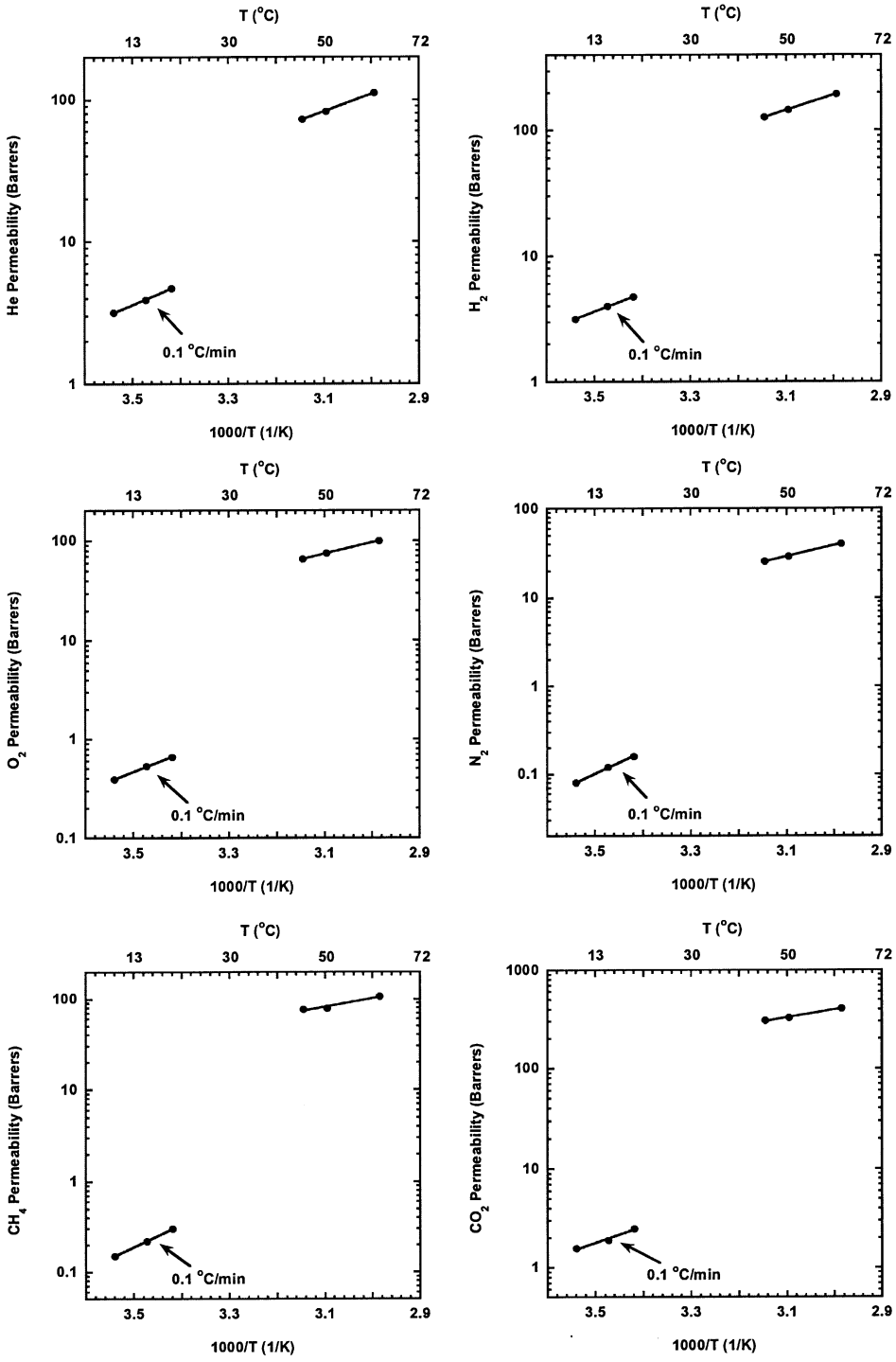


Fig. 3. He, $H_2$, $O_2$, $N_2$, $CH_4$, and $CO_2$ permeability (Barrers) of poly(octadecyl methacrylate) (PMA-18) as a function of temperature.

with different membrane areas and thicknesses. The maximum error was 4% for $N_2$ at 40°C (% error = 100 × S.D./avg.). A PPO coated ceramic porous support was used here and requires a smaller correction than the PE film in the prior study. The permeance of each support material was accounted for and subtracted from the composite permeance [48,50]. Errors in thickness measurement or membrane defects may cause this discrepancy. Thus, we feel confident that the margin of error in the PA-1 results is small and that the trends seen in Figs. 5 and 6 are quite real.

Table 4 compares permeability coefficients for rubbery PA-1 and PA-2 with the corresponding glassy polymethacrylates, PMA-1 = poly(methyl methacrylate) and PMA-2 = poly(ethyl methacrylate), at 35°C using reliable data

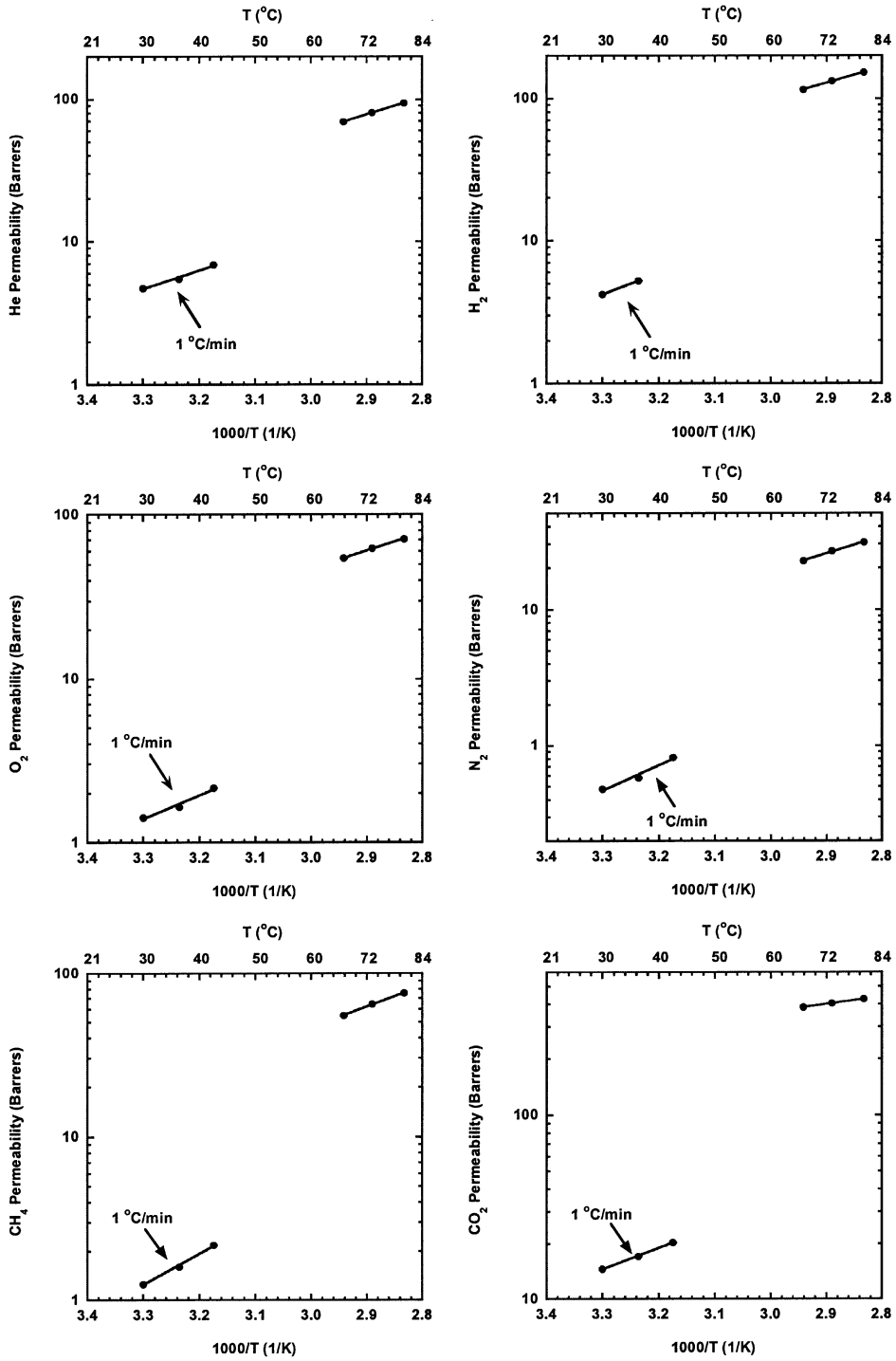


Fig. 4. He, $H_2$, $O_2$, $N_2$, $CH_4$, and $CO_2$ permeability (Barrers) of polycaprolactone (PCL) as a function of temperature.

from the literature [51,52]. We see that the ratio PA-2/PA-1 and PMA-2/PMA-1 are of similar magnitude for a given gas and in general, both ratios increase rather strongly as the diameter of the gas molecule increases. Of course, as expected, the absolute values of PA-1 are much higher than those of PMA-1 especially for the larger gases; the same trend is seen for PA-2 versus PMA-2.

As the alkyl side-chain becomes very long, one might expect the permeability to approach the value for amorphous polyethylene. The arithmetic scale in Fig. 5 does not seem to support an asymptote; however, the logarithmic scale used in Fig. 6 makes an asymptote seem more plausible. There are no direct measurements of the gas permeability of amorphous polyethylene; thus it is not possible to

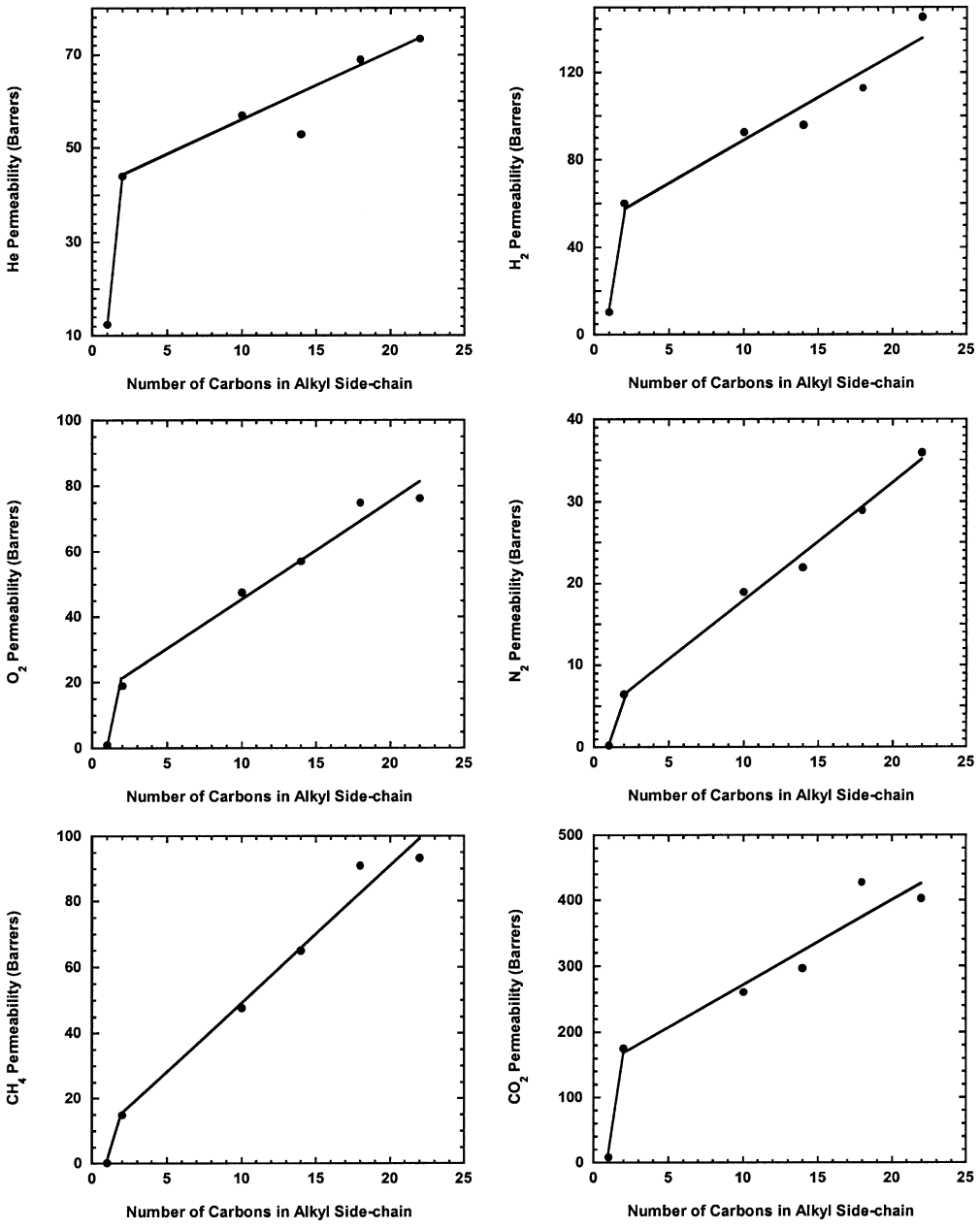


Fig. 5. He, $H_2$, $O_2$, $N_2$, $CH_4$, and $CO_2$ permeability (Barrers) of amorphous poly(alkyl acrylate)s as a function of side-chain length at 35°C on an arithmetic scale.

Table 4
The permeability change of both glassy and rubbery poly(alkyl (meth)acrylate)s upon addition of the first methylene. All values given at 35°C in Barrers

| Polymer | He | $H_2$ | $O_2$ | $N_2$ | $CH_4$ | $CO_2$ |
|---|---|---|---|---|---|---|
| PMA-1[a] | 9.2 | 6.3 | 0.096 | 0.0135 | 0.0058 | 0.36 |
| PMA-2[b] | 23.8 | 21.8 | 1.86 | 0.326 | 0.347 | 7.01 |
| $P_{PMA-2/PMA-1}$ | 2.6 | 3.5 | 19.4 | 24.1 | 59.8 | 19.5 |
| PA-1 | 12.4 | 10.6 | 1.06 | 0.236 | 0.288 | 9.58 |
| PA-2 | 44 | 60.4 | 19 | 6.5 | 14.9 | 176 |
| $P_{PA-2/PA-1}$ | 3.5 | 5.7 | 17.9 | 27.5 | 51.7 | 18.3 |

[a] From Ref. [51].
[b] From Ref. [52].

unambiguously evaluate this proposal. Table 5 lists data from the literature that might represent reasonable analogs for amorphous polyethylene. The permeability coefficients for a given gas sometimes vary significantly among these various hydrocarbon rubbers suggesting that it is difficult to infer the permeability of amorphous polyethylene in this way. However, it is important to note that, for any given gas, the permeability of molten PA-22 is higher than the values listed for the various hydrocarbon rubbers shown in Table 5. Thus, it appears that the permeability of poly(alkyl acrylate)s at very long alkyl side-chain length exceeds that of amorphous

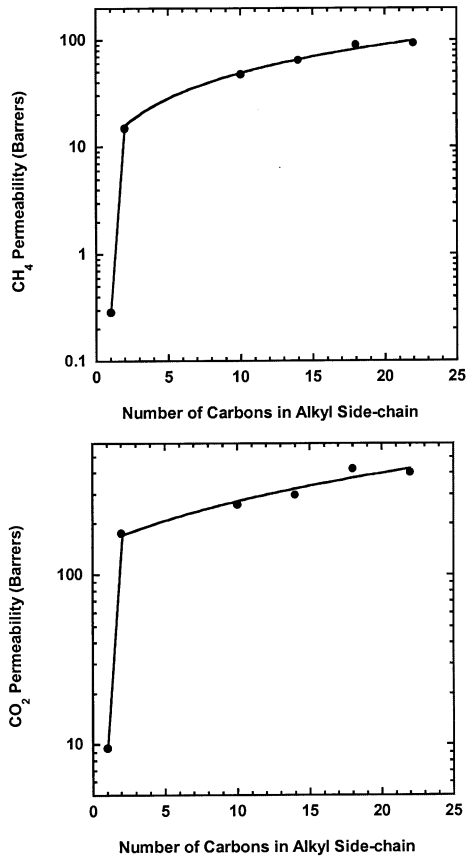


Fig. 6. $CH_4$ and $CO_2$ permeability (Barrers) of amorphous poly(alkyl acrylate)s as a function of side-chain length at 35°C on a logarithmic scale.

polyethylene unless the permeability of the latter is much higher than the data in Table 5 tend to suggest. It would be interesting to explore this issue with more definitive experiments.

### *4.4. Gas permeability of semi-crystalline poly(alkyl acrylate)s*

The gas permeability in the semi-crystalline state of these polymers depends on some properties that are easily characterized and others that are not. The amorphous phase permeability, extent of chain immobilization, and the degree of crystallinity have somewhat quantifiable effects on the permeation properties in the semi-crystalline state. However, the effect of physical structure such as the crystallite size, shape, orientation, and distribution on the permeation properties is much harder to quantify and has a great influence on the overall transport characteristics for the polymers studied here.

The gas permeability coefficients for the poly(alkyl acrylate)s in the semi-crystalline state are shown in Table 6. It is instructive to examine trends in Table 6 for PA-14, PA-18, and PA-22 films cooled at 0.1°C/min. As expected, crystallinity increases as the side-chain becomes longer which tends to decrease the permeability. The permeability of PA-14 is higher than that of PA-18; however, for PA-22 the permeability is higher than for PA-18. Chain immobilization of the amorphous state by the crystals is no doubt also a factor in these trends. The higher degree of crystallinity in the longer side-chain polymers may lead to higher $\beta$ values, thereby reducing the amorphous permeability. The effect of this immobilization factor on transport properties will be explained further in a subsequent section. Of course, there are competing effects in these side-chain crystalline materials. As the side-chain length increases, the amorphous state permeability increases (see Fig. 5) but longer side-chains also lead to an increase in the crystallinity and possibly $\beta$. The size (especially aspect ratio) and arrangement of the crystals, in addition to crystallinity, can also have an important effect on permeability, and, unfortunately, currently available

Table 5
Comparison of gas permeability coefficients for molten or rubbery state polymers considered as candidates for the amorphous analog of polyethylene. All values given at 35°C in Barrers

| Polymer | He | $H_2$ | $O_2$ | $N_2$ | $CH_4$ | $CO_2$ | Reference |
|---|---|---|---|---|---|---|---|
| PA-22 | 73.5 | 146 | 76.3 | 36.0 | 93.4 | 404 | This work |
| Natural rubber | 43.3 | 71.1 | 36.2 | 13.1 | 28.9 | 183 | [60] |
| Methyl rubber | – | 26.4 | 3.90 | 1.00 | – | 13.9 | [60] |
| Butyl rubber | 12.7 | 11.8 | 2.30 | 0.70 | – | 8.9 | [60] |
| Molten gutta percha | – | 87.3 | 46.1 | 15.0 | – | 226 | [60] |
| Polybutadiene | – | 61.4 | 27.6 | 10.2 | – | 177 | [60] |
| Molten polybutadiene (48% *trans*) | – | 9.10 | – | 2.30 | – | 31.4 | [26] |
| Poly(*cis*-4-butadiene) | 42.9 | – | – | 25.1 | – | – | [61] |
| Ethylene/propylene rubber (47/53) | 28.6 | – | – | 7.50 | – | – | [61] |
| Ethylene/propylene rubber (37/63) | 43.5 | – | – | 10.3 | – | – | [61] |
| Ethylene/propylene rubber (29/71) | 46.0 | – | – | 8.70 | – | – | [61] |
| Molten polyethylene[a] | – | – | – | 152 | – | 249 | [62,63] |
| Molten polypropylene[a] | – | – | – | – | – | 540 | [62,63] |

[a] The permeability was calculated at 35°C using the reported values of $D$, $S$, $E_d$, and $\Delta H_s$.

Table 6
Comparison of gas permeability coefficients ($P$), activation energies for gas permeation ($E_p$), chain immobilization factors ($\beta_r$) relative to He at given temperatures, and activation energies of the chain immobilization factor ($E_\beta$) expressed as absolute values for semi-crystalline poly(alkyl acrylate)s, poly(octadecyl methacrylate), and PCL

| Polymer | Thermal history (°C/min)[a] | $\alpha$ | | He | $H_2$ | $O_2$ | $N_2$ | $CH_4$ | $CO_2$ |
|---|---|---|---|---|---|---|---|---|---|
| PA-14 | 0.1 | 0.76 | $P$[b] | 12.2 | 14.9 | 6.62 | 2.17 | 4.45 | 21.3 |
| | | | $E_p$[c] | 6.1 | 6.4 | 8.7 | 10.1 | 8.6 | 6.6 |
| | | | $\beta_r$ (25°C) | – | 1.5 | 2.3 | 2.8 | 3.7 | 3.7 |
| | | | $\lvert E_\beta \rvert$[c] | 0.4 | 0.7 | 3.0 | 3.5 | 2.1 | 2.8 |
| PA-18 | 1.0 | 0.63 | $P$ | 8.24 | 8.35 | 1.18 | 0.29 | 0.64 | 4.25 |
| | | | $E_p$ | 7.4 | 8.0 | 11.2 | 12.6 | 13.1 | 9.2 |
| | | | $\beta_r$ (50°C) | – | 1.7 | 5.6 | 8.3 | 11.3 | 8.5 |
| | | | $\lvert E_\beta \rvert$ | 2.0 | 1.7 | 6.0 | 6.3 | 7.5 | 6.5 |
| PA-18 | 0.1 | 0.59 | $P$ | 9.01 | 9.78 | 1.87 | 0.54 | 1.23 | 6.98 |
| | | | $E_p$ | 6.4 | 7.3 | 9.3 | 10.8 | 9.9 | 7.7 |
| | | | $\beta_r$ (50°C) | – | 1.5 | 4.2 | 5.5 | 7.5 | 6.0 |
| | | | $\lvert E_\beta \rvert$ | 1.0 | 1.0 | 4.1 | 4.5 | 4.3 | 5.0 |
| PA-22 | 1.0 | 0.53 | $P$ | 7.58 | 7.97 | 1.55 | 0.49 | 1.09 | 6.01 |
| | | | $E_p$ | 6.5 | 7.0 | 7.7 | 8.7 | 8.3 | 5.9 |
| | | | $\beta_r$ (70°C) | – | 1.6 | 3.9 | 5.1 | 6.4 | 5.4 |
| | | | $\lvert E_\beta \rvert$ | 2.1 | 2.4 | 2.9 | 3.8 | 5.4 | 5.9 |
| PA-22 | 0.1 | 0.50 | $P$ | 9.36 | 9.83 | 2.00 | 0.63 | 1.50 | 7.75 |
| | | | $E_p$ | 7.1 | 7.9 | 8.7 | 9.8 | 9.2 | 6.6 |
| | | | $\beta_r$ (70°C) | – | 1.5 | 3.5 | 4.6 | 5.5 | 5.2 |
| | | | $\lvert E_\beta \rvert$ | 2.2 | 3.5 | 4.1 | 5.0 | 4.3 | 3.7 |
| PMA-18 | 0.1 | 0.76 | $P$ | 8.25 | 8.45 | 1.40 | 0.43 | 0.80 | 4.68 |
| | | | $E_p$ | 6.5 | 6.7 | 8.7 | 11.4 | 11.4 | 7.6 |
| | | | $\beta_r$ (45°C) | – | 1.7 | 4.8 | 5.2 | 8.2 | 7.0 |
| | | | $\lvert E_\beta \rvert$ | 0.8 | 1.0 | 3.5 | 5.7 | 7.0 | 3.9 |
| PCL | 1.0 | 0.58 | $P$ | 5.48 | 5.06 | 1.66 | 0.59 | 1.57 | 16.8 |
| | | | $E_p$ | 5.9 | 6.8 | 6.5 | 8.4 | 8.7 | 5.3 |
| | | | $\beta_r$ (67°C) | – | 1.6 | 2.3 | 2.1 | 1.8 | 2.0 |
| | | | $\lvert E_\beta \rvert$ | 0.3 | 1.6 | 1.5 | 2.7 | 2.9 | 3.4 |

[a] Rate of cooling from the melt.
[b] $P$ is measured at or extrapolated to 35°C and has units of Barrers.
[c] $E_p$ and $E_\beta$ have units of kcal/mol; $E_\beta = E_a - E_c$, where $E_a$ and $E_c$ are the activation energies of permeation for the amorphous and crystalline states.

techniques do not allow full determination of these factors. These factors are strongly influenced by thermal history.

The effect of thermal history on permeability is illustrated in Fig. 7, where the permeability of materials cooled from the melt at different rates is compared. The trends for PA-18 and PA-22 are similar. Rapid cooling (1.0°C/min) leads to significantly lower permeability than slower cooling (0.1°C/min) even though rapid cooling leads to slightly less crystallinity. When comparing these thermal histories for PA-22, the permeability is changed by roughly the same percentage for a given penetrant, see Table 6. This is in contrast with PA-18 for which the larger penetrants are affected more than the smaller ones. The effect of thermal history on the activation energy, see Table 6, depends on the polymer. An increase in crystallinity leads to higher $E_p$ for PA-22, as would be expected, but $E_p$ decreases for PA-18.

### 4.5. Polycaprolactone

Measurement of the permeability of a main-chain crystalline polymer in both the amorphous and crystalline states was of interest for this work to determine whether the magnitude of the permeation switch and its dependence on penetrant size is unique to side-chain crystalline polymers. The literature offers no well-defined examples for this comparison. In two cases, the crystallinity of the materials investigated is not reported [25,28]. This is a factor of paramount importance in the magnitude of the permeation switch effect. The permeation switch for polyethylene cannot be assessed directly because data for amorphous polyethylene are not available; however, an amorphous analog, like natural rubber could be used to provide an estimate. PCL was chosen for these experiments for a number of reasons. First, and foremost, this polymer has a melting point that is low enough so that the molten state properties can be conveniently measured in our permeation apparatus. Second, the crystallinity is similar to that of the side-chain polyacrylates when compared at similar thermal history. Last, PCL has a chemical structure somewhat similar to the acrylates.

The gas permeability coefficients for amorphous PCL are of the same order of magnitude as the poly(alkyl acrylate)s, as seen in Table 3. PCL is a structural isomer of poly(propyl acrylate) (PA-3), whose gas permeation properties have

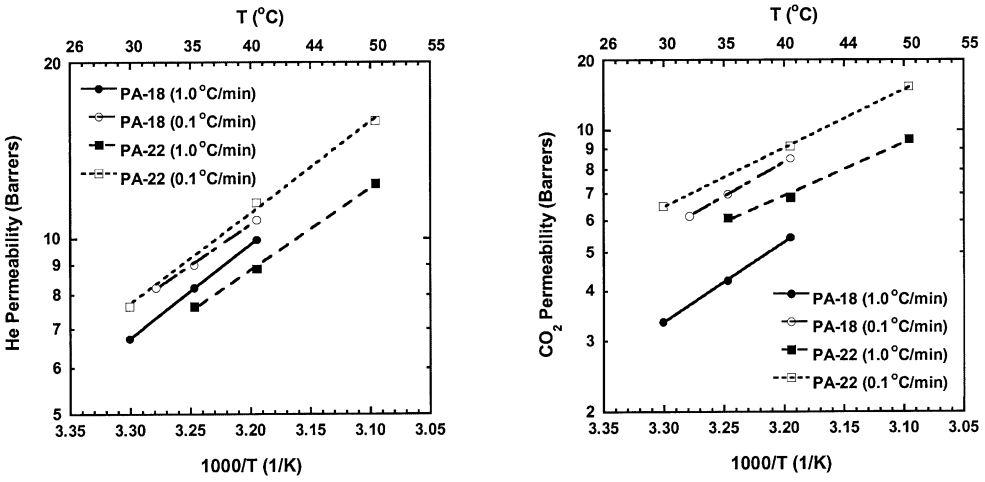


Fig. 7. He and $CO_2$ permeability (Barrers) as a function of temperature in the semi-crystalline state for different thermal histories of PA-18 and PA-22.

been interpolated by the best fit lines in Fig. 5. The gas permeability coefficients for PA-3 are very similar to those of PCL with the only significant differences being for He and $CO_2$. Of course, the chain packing of these structural isomers cannot be expected to be exactly the same [53]. Except for PA-1, the acrylates have similar activation energies as PCL, see Table 3.

Table 6 shows PCL ($\alpha = 0.58$) to have higher crystalline state permeabilities than PA-18 ($\alpha = 0.59$) with the exception of He and $H_2$. The $O_2$ and $N_2$ permeation properties of semi-crystalline PCL were recently reported, and despite differences in thermal history (similar $\alpha$), there is good agreement with the values presented here [54]. Lower activation energies were observed for PCL ($\alpha = 0.58$) compared to PA-18 ($\alpha = 0.59$) as seen in Table 6.

### 4.6. Permeation switch: main versus side-chain crystallinity

The permeation switch effect as defined here, $P_T^+/P_T^-$, depends on both the molten and semi-crystalline state permeabilities and the reference temperature at which this evaluation is made. It is important to note that extrapolations from the melt and crystalline state were made based on the Arrhenius fit of the temperature dependent permeation data. This is especially important in the semi-crystalline state, where melting of the crystals can lead to dramatic changes in permeability. It was assumed that where the Arrhenius fit applied, no pre-melting of the crystals was occurring, i.e. the data were taken sufficiently far from the melting point that the overall crystalline morphology is fixed. The choice of reference temperature significantly affects the permeation switch value because the activation energies of permeation are not the same in the molten and semi-crystalline states. The activation energy is greater in the semi-crystalline state than in the molten state; thus, the value of the permeation switch is smaller the higher the selected reference temperature. In what follows we will summarize, to the extent possible, each of the factors that contribute to the magnitude of the switch effect.

Fig. 8 shows the permeation switch values as a function of the penetrant size for PA-14, PA-18 (from Ref. [18]), and PA-22 for films cooled from the melt at 0.1°C/min. The reference temperature is different for each polymer and corresponds closely to the melting point of each material. As reported previously, the values of the permeation switch depends strongly on the size of the penetrant. The Lennard–Jones and kinetic diameters are very similar for the gases studied here except for $CO_2$; whose kinetic diameter is smaller, 3.3 Å, owing to its more cylindrical shape. Relative to the line defined by the other gases, $CO_2$ falls below when plotted at its Lennard–Jones diameter or above when plotted at its kinetic diameter. An intermediate choice of

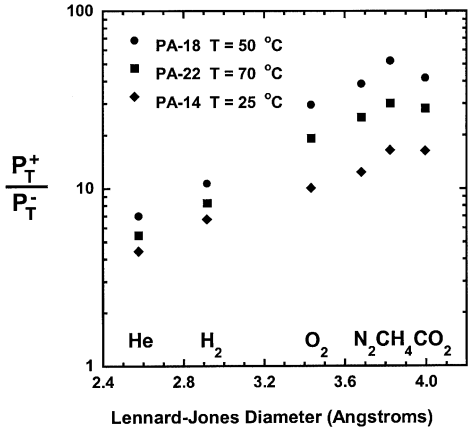


Fig. 8. Magnitude of the permeation switch as a function of the Lennard–Jones collision gas diameter for poly(alkyl acrylate)s. Note that if the kinetic diameters were used instead, the location of the $CO_2$ point would shift to the left and lie above the trend for the other gases. The thermal history of the semi-crystalline state for these polymers was established by cooling from the melt at 0.1°C/min. The permeation switch temperature, $T$, is approximately the melting point of the polymer. $\alpha_{PA-18} = 0.59$, $\alpha_{PA-22} = 0.50$, $\alpha_{PA-14} = 0.76$.

dimension might be more appropriate; however, the point here is that the permeation switch depends on the penetrant.

This size dependence has been interpreted to be a result of constraints on the amorphous phase caused by the crystals, i.e. chain immobilization effect [18]. While the parameter, $\beta$, that describes this effect in Eq. (3) cannot be isolated without a value for $\tau$, the value of $\beta$ relative to another penetrant can be determined and the temperature dependence of $\beta$ can be evaluated.

For the model described earlier, the permeation switch, or the ratio of the amorphous ($P_a$) to semi-crystalline state ($P_c$) permeability, is equal to $\tau\beta/\alpha$ at a particular temperature. Since $\tau$ and $\alpha$ are independent of the penetrant, a ratio of the permeation switch for gas X to He is described by

$$\left(\frac{P_a}{P_c}\right)_X \Big/ \left(\frac{P_a}{P_c}\right)_{He} = \frac{\beta_X}{\beta_{He}} = \beta_r. \quad (5)$$

In their analysis of data for polyethylene, Michaels and Bixler assumed that natural rubber is a suitable analog of completely amorphous polyethylene and that $\beta_{He} = 1$ and then calculated values of $\beta$ for the other penetrants [21]. Certainly, these two assumptions are open to question. Table 6 shows values of $\beta$ relative to He, i.e. $\beta_r$, for all the materials of interest here as calculated by Eq. (5). The switch magnitudes shown in Fig. 8 mirror the calculated $\beta$ ratios; e.g. in addition to the size dependence, $\beta_r$ is larger for PA-18 than PA-14 but the ratio for PA-22 is smaller than PA-18, consistent with the figure. Cooling PA-18 and PA-22 at a slower rate from the melt leads to a lower $\beta_r$ despite the increase in crystallinity. This is consistent with the observation illustrated in Fig. 7, where it is shown that cooling at 1.0°C/min leads to a higher permeability than cooling at 0.1°C/min.

The temperature dependence of $\beta$ can be analyzed by examining how the permeation switch depends on temperature

$$P_c(T)/P_a(T) = \alpha/\tau\beta(T). \quad (6)$$

Far removed from the melting point, both $\tau$ and $\alpha$ should be independent of temperature. Assuming a typical Arrhenius temperature dependence for $\beta$, such that

$$\beta \sim \exp\left(\frac{-E_\beta}{RT}\right) \quad (7)$$

eliminating the $\tau$ and $\alpha$ terms, and simplifying yields

$$E_\beta = E_a - E_c, \quad (8)$$

where $E_a$ and $E_c$ are the activation energies of permeation in the amorphous and crystalline states. Note that $E_\beta$ is always $<0$ for the polymers presented here. This means that far removed from the melting point, $\beta$ becomes larger the lower the temperature. Interpreting the trends in $E_\beta$ among penetrants and polymers in a facile manner necessitates using the absolute value of $E_\beta$, seen in Table 6. Generally, $|E_\beta|$ increases with increasing penetrant size, somewhat similar to the trend seen for the permeation switch. At similar thermal history and for a given penetrant, $|E_\beta|$ increases going from PA-14 to PA-18 but shows mixed behavior from PA-18 to PA-22. For different thermal histories for the same polymer, mixed trends persist; $E_\beta$ decreases when going from 1.0 to 0.1°C/min for PA-18 but increases in the case of PA-22.

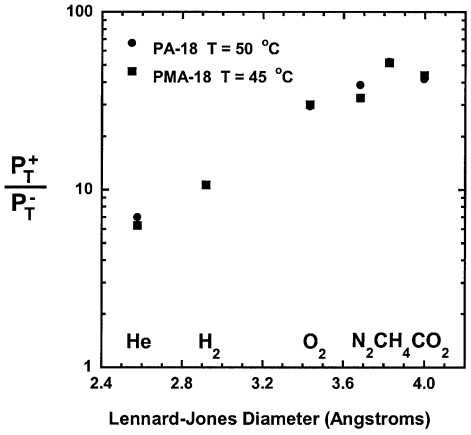


Fig. 9. Magnitude of the permeation switch for poly(octadecyl acrylate) (PA-18) and poly(octadecyl methacrylate) (PMA-18) at the melting point as a function of the Lennard–Jones collision gas diameter. The thermal history of the semi-crystalline state for these polymers was established by cooling from the melt at 0.1°C/min. $\alpha_{PA-18} = 0.59$, $\alpha_{PMA-18} = 0.76$.

PA-18 has a larger switch than PA-14, in part due to a higher degree of crystallinity. PA-22 displays anomalous behavior with a switch lower than PA-18 but can be explained somewhat with the analysis of the chain immobilization factor above. Again, the interplay and counteracting effects of side-chain length on both amorphous phase permeability and crystalline morphology are factors in the trends seen here.

The effect of backbone stiffness on the permeation switch is shown in Fig. 9. Poly(octadecyl methacrylate) (PMA-18) and PA-18 were cooled from the melt at 0.1°C/min to establish a fixed thermal history. Despite the large difference in crystallinity between the two polymers, the switch values are practically the same at the temperatures shown. Table 7 compares the absolute permeability coefficients for PA-18 and PMA-18 in the molten and semi-crystalline states at 50°C. The lower amorphous permeability of PMA-18 compared to PA-18 might be expected based on the differences in backbone rigidity. The reduced permeability in

Table 7
Comparison of gas permeability coefficients for poly(octadecyl acrylate) (PA-18) and poly(octadecyl methacrylate) (PMA-18) in the crystalline and molten state illustrating the effect of backbone stiffness. All values given at 50°C in Barrers

| Polymer | State | He | $H_2$ | $O_2$ | $N_2$ | $CH_4$ | $CO_2$ |
|---|---|---|---|---|---|---|---|
| PA-18 | Crystalline | 14.8 | 17.1 | 3.76 | 1.22 | 2.64 | 12.5 |
| PMA-18 | Crystalline | 13.5 | 14.0 | 2.71 | 1.03 | 1.90 | 8.33 |
| PA-18 | Molten | 104 | 183 | 111 | 47.0 | 138 | 524 |
| PMA-18 | Molten | 83.4 | 146 | 74.8 | 29.3 | 82.7 | 332 |

both the amorphous and crystalline states, stemming from differences in crystal structure, backbone stiffness, and morphology for PMA-18 leads to a coincidental overlap in permeation switch values at the temperatures specified.

The magnitude of the permeability switch effect for these polymers also includes a compositional change at the melting point that has not been accounted for. The amorphous phase of the semi-crystalline polymer includes only ten or so of the methylene groups. However, above $T_m$, all of the methylene units of the alkyl side-chain are included in the amorphous phase. The effect of this compositional change can be accounted for in the following approximate way. Poly(decyl acrylate) (PA-10) is completely amorphous and has 10 side-chain methylene units; thus, the permeability of PA-10 at 50°C should provide an estimate of the $P_{50}^{+}$ value for PA-18 in the *absence* of this compositional change. The $P_{50}^{+}$ values for PA-18 and for PA-10 are shown in Table 8. The latter $P_{50}^{+}$ value is used to estimate the compositionally corrected $P_{50}^{+}/P_{50}^{-}$ ratio. As seen in Table 8, the compositional change accounts for 20–40% of the permeation jump actually observed.

Fig. 10 compares the permeation jump for PCL and PA-18 with the same thermal history and similar degree of crystallinity. Clearly, PCL does not experience a composition change as the entire backbone can participate in the crystal formation. The permeation jump values for PCL are lower and less penetrant dependent than those of PA-18. The small effect of penetrant size on the permeation jump of PCL seems to be characteristic of main-chain polymers. *Trans*-polybutadiene [26], polyethylene (using natural rubber as the amorphous analog) [18,21], filled silicone rubber (semi-crystalline at −50°C) [25], and *trans*-poly(isoprene) or gutta percha [28] show similar behavior. Chain immobilization of the amorphous phase by crystallites seems to have less effect on gas transport for these main-chain polymers.

The contribution of the composition change estimated in Table 8 for PA-18, while significant, does not fully explain the difference in the magnitudes of the permeation jumps seen in Fig. 10. We think the difference is due to an inherently larger extent of constraints in side-chain polymers

Table 8
The poly(octadecyl acrylate) permeability dependence on composition caused by melting of the side-chain crystals. Permeability values are in Barrers. The semi-crystalline state has been cooled from the melt at 1.0°C/min ($\alpha = 0.63$)

| Permeability or permeability jump | He | $H_2$ | $O_2$ | $N_2$ | $CH_4$ | $CO_2$ |
|---|---|---|---|---|---|---|
| $P_{50}^{+}$ (PA-18) | 104 | 183 | 112 | 47.0 | 138 | 524 |
| $P_{50}^{+}$ (PA-10) | 84.9 | 139 | 75.5 | 29.1 | 83.0 | 345 |
| $P_{50}^{+}$ (PA-18)/$P_{50}^{-}$ (PA-18) | 7.2 | 12.0 | 40.0 | 59.6 | 81.5 | 61.1 |
| $P_{50}^{+}$ (PA-10)/$P_{50}^{-}$ (PA-18) | 5.9 | 9.1 | 27.1 | 36.9 | 48.8 | 40.3 |
| Composition contribution to switch effect (%) | 18 | 24 | 32 | 38 | 40 | 34 |

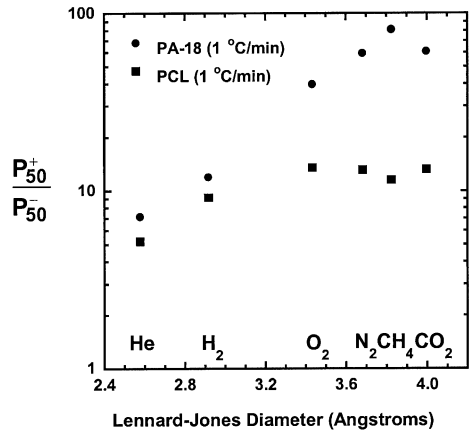


Fig. 10. Magnitude of the permeation switch of PCL and PA-18 at 50°C as a function of the Lennard–Jones collision gas diameter. The thermal history of the semi-crystalline state for these polymers was established by cooling from the melt at 1°C/min. $\alpha_{PA-18} = 0.63$, $\alpha_{PCL} = 0.58$.

compared to main-chain polymers. We attempt to depict this view in Fig. 11 [10,55–57]. The dashed lines show the somewhat arbitrary boundary between the crystalline and amorphous regions of the polymer. The amorphous phase of the main-chain polymer consists of loops that re-enter the same crystal, tie-chains that connect adjacent crystals, and dangling chain ends. By comparison, these chains would seem to have far more conformational (or motional) degrees of freedom than those in the amorphous phase of the side-chain crystalline polymer where the backbone is connected to the crystalline regions on every other carbon atom

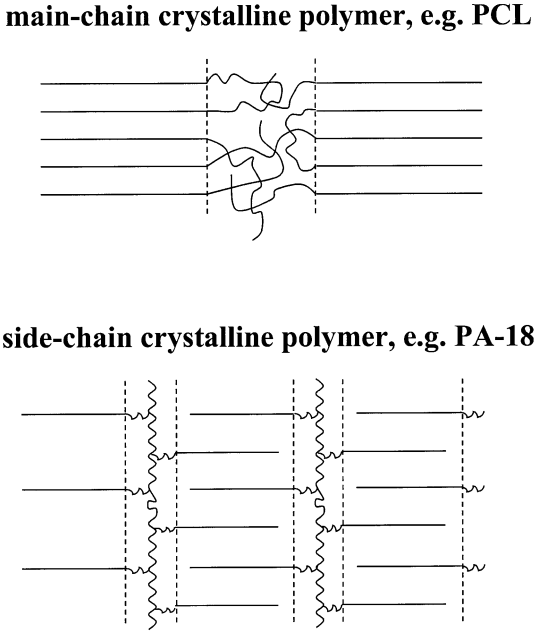


Fig. 11. Schematic representation of the crystalline state for main- and side-chain crystalline polymers illustrating the differences in the amorphous phases for the two polymer classes. The separation between the crystalline and amorphous regions is given by the dashed lines.

(through about 10 methylene units). Thus, it appears to us that there is a greater constraint on the amorphous phase in the side-chain material. The proposed high level of motional constraint of the 'amorphous' phase of the side-chain material (i.e. the backbone plus a portion of the alkyl unit, as suggested in Fig. 11) is supported by the recent studies of the dielectric relaxation behavior for poly(octadecyl methacrylate) in both the semi-crystalline and molten states reported by Alig et al. [56]. The ester group is dielectrically active and resides in the amorphous phase regardless of the temperature; thus, its relaxation behavior reflects the mobility of the backbone and the amorphous phase. A large relaxation peak, associated with the ester group, is quite prominent above $T_m$ but effectively disappears below $T_m$. Thus, these authors conclude that the side-chain crystals very effectively immobilize the backbone and, hence, the amorphous phase in the semi-crystalline state of this polymer [56].

Of course, limitations of the two-phase model for semi-crystalline polymers are apparent. There is no clear demarcation between the amorphous and crystalline phases as shown by recent studies on the phase mobility of main-chain semi-crystalline polymers using solid-state NMR [57–59]. The presence of an interfacial region has been detected with a reduced mobility compared to bulk amorphous regions [57–59]. Such experiments do not appear to have been reported for side-chain crystalline poly(alkyl (meth)acrylate)s. In addition, owing to the kind of motional constraints suggested in Fig. 11, even the amorphous phase cannot be expected to have the properties (especially transport) of a free amorphous phase. Empirically, both issues may be lumped into a chain immobilization factor as suggested by Michaels and Bixler as described above.

## 5. Conclusions

The amorphous and semi-crystalline state permeability and the permeation switch are significantly influenced by the side-chain length of the poly(alkyl acrylate)s. Chemical structure effects were observed in the amorphous state where an increase in permeability occurred as the side-chain was lengthened. The alkyl substituent led to varying degrees of crystallinity and possibly different thermal history dependent morphologies. The mixed trends in the crystalline state were also manifest in the permeation switch magnitudes. The penetrant dependent permeation switch for PA-14 and PA-22 followed the same trend as PA-18, which is thought to be based in chain immobilization of the amorphous state. The stiffer backbone of PMA-18 compared to PA-18 resulted in similar permeation switch values. The composition change at the melting point did not account for the difference in permeation switch magnitudes between PA-18 and PCL. It is believed that differences in crystal structure, crystalline morphology, and a constrained amorphous state contribute to this phenomenon.

## Acknowledgements

This research was funded by National Science Foundation grant number CTS 97-14305 administered by the Division of Chemical and Transport Systems — Separation and Purification Processes Program.

## References

[1] Jordan EF, Feldeisen DW, Wrigley AN. J Polym Sci Part A-1 1971;9:1835–52.
[2] Jordan EF, Artmyshyn B, Speca A, Wrigley AN. J Polym Sci Part A-1 1971;9:3349–65.
[3] Jordan EF. J Polym Sci Part A-1 1971;9:3367–78.
[4] Jordan EF, Riser GR, Artmyshyn B, Pensabene JW, Wrigley AN. J Polym Sci Part A-2 1972;10:1657–79.
[5] Platé NA, Shibaev VP. Comb-shaped polymers and liquid crystals. New York: Plenum Press, 1987.
[6] Platé NA, Shibaev VP. J Polym Sci. Macromol Rev 1974;8:117–253.
[7] Platé NA, Shibaev VP, Petrukhin BS, Zubov YA, Kargin VA. J Polym Sci Part A-1 1971;9:2291–8.
[8] Platé NA, Shibaev VP, Petrukhin BS, Kargin VA. J Polym Sci Part C 1968;23:37–44.
[9] Rehberg CE, Fisher CH. J Am Chem Soc 1944;66:1203–7.
[10] Hsieh HWS, Post B, Morawetz H. J Polym Sci: Polym Phys. 1976;14:1241–55.
[11] Hirabayashi T, Yokota K. Polym J 1987;19:1115–9.
[12] Hirabayashi T, Kikuta T, Kasabou K, Yokota K. Polym J 1988;20:693–8.
[13] Kricheldorf HR, Domschke A. Macromolecules 1996;29:1337–44.
[14] Magagnini PL, Tassi EL, Andruzzi F, Paci M. Polym Sci 1994;36:1502–15.
[15] Tsujita Y, Ojika R, Takizawa A, Kinoshita T. J Polym Sci: Part A: Polym Chem 1990;28:1341–51.
[16] Greene L, Phan LX, Mohr JM. Side-chain crystallizable polymers for temperature-activated controlled release. In: El-Nokaly MA, Piatt DM, Charpentier BA, editors. Polymeric delivery systems properties and applications, vol. 520. Washington, DC: American Chemical Society, 1993.
[17] Stewart RF, Mohr JM, Budd EA, Phan LX, Arul J. Temperature-compensating films for modified atmosphere packaging of fresh produce. In: El-Nokaly MA, Pratt DM, Charpentier BA, editors. Polymeric delivery systems: properties and applications, vol. 520. Washington, DC: American Chemical Society, 1993.
[18] Mogri Z, Paul DR. Polymer 2001;42:2533–44.
[19] Michaels AS, Parker RB. J Polym Sci 1959;41:53–71.
[20] Michaels AS, Bixler HJ. J Polym Sci 1961;50:393–412.
[21] Michaels AS, Bixler HJ. J Polym Sci 1961;50:413–39.
[22] Michaels AS, Vieth WR, Barrie JA. J Appl Phys 1963;34:1–12.
[23] Michaels AS, Vieth WR, Barrie JA. J Appl Phys 1963;34:13–20.
[24] Michaels AS, Bixler HJ, Fein HL. J Appl Phys 1964;35:3165–78.
[25] Barrer RM, Chio HT. J Polym Sci: Part C 1965;10:111–38.
[26] Cowling R, Park GS. J Membr Sci 1979;5:199–207.
[27] Lowell PN, McCrum NG. J Polym Sci Part A-2 1971;9:1935–54.
[28] Van Amerongen GJ. J Polym Sci 1947;2:381–6.
[29] Luyten MC, van Ekenstein GORA, ten Brinke G, Ruokolainen J, Ikkala O, Torkkeli M, Serimaa R. Macromolecules 1999;32:4404–10.
[30] Inomata K, Sakamaki Y, Nose T, Sasaki S. Polym J 1996;28:992–9.
[31] Paul DR, Yampol'skii YP, editors. Polymeric gas separation membranes. Boca Raton: CRC Press, 1994.
[32] Koros WJ, editor. Barrier polymers and structures. Washington, DC: American Chemical Society, 1990.

[33] Ho WSW, Sirkar KK, editors. Membrane handbook New York: Van Nostrand Reinhold, 1992.
[34] Kesting RE, Fritzsche AK. Polymeric gas separation membranes. New York: Wiley, 1993.
[35] Morisato A, He Z, Pinnau I. Polym Prepr (Am Chem Soc, Polym Mat Sci and Engng) 1999;81:529–30.
[36] Masuda T, Iguchi Y, Tang B-Z, Higashimura T. Polymer 1988;29:2041–9.
[37] Masuda T, Matsumoto T, Yoshimura T, Higashimura T. Macromolecules 1990;23:4902–7.
[38] Savoca AC, Surnamer AD, Tien C-F. Macromolecules 1993;26:6211–6.
[39] Takada K, Matsuya H, Masuda T, Higashimura T. J Appl Polym Sci 1985;30:1605–16.
[40] Krizan TD, Coburn JC, Blatz PS. Structure of amorphous polyamides. In: Koros WJ, editor. Barrier polymers and structures, vol. 423. Washington, DC: American Chemical Society, 1990.
[41] Gray DN. Polym Engng Sci 1977;17:719–23.
[42] Wisian-Neilson P, Xu G. Macromolecules 1996;29:3457–61.
[43] Dorkenoo KD, Pfromm PH, Rezac ME. J Polym Sci Part B Polym Phys 1998;36:797–803.
[44] Kawakami Y, Toda H, Higashino M, Yamashita Y. Polym J 1988;20:285–92.
[45] Matsumoto A, Oki Y, Otsu Y. Makromol Chem Rapid Commun 1990;11:507–12.
[46] Matsumoto A, Oki Y, Otsu Y. Polym J 1991;23:201–9.
[47] Simril VL. J Polym Sci 1947;2:142–56.
[48] Mogri Z, Paul DR. J Membr Sci. 2000;175:253–65.
[49] Van Krevelen DW. Properties of polymers. 3rd ed. New York: Elsevier, 1990.
[50] Chiou JS, Barlow JW, Paul DR. J Appl Polym Sci 1985;30:1173–86.
[51] Raymond PC, Paul DR. J Polym Sci Part B Polym Phys 1990;28:2079–102.
[52] Chiou JS, Paul DR. J Membr Sci 1989;45:167–89.
[53] Burgess WH, Hopfenberg HB, Stannett VT. J Macromol Sci Phys 1971;5:23–40.
[54] Ng CS, Teoh SH, Chung TS, Hutmacher DW. Polymer 2000;41:5855–64.
[55] Allcock HR, Lampe FW. Contemporary polymer chemistry. 2nd ed. Englewood Cliffs, NJ: Prentice-Hall, 1990.
[56] Alig I, Jarek M, Hellmann GP. Macromolecules 1998;31:2245–51.
[57] Kitamaru R, Horii F, Murayama K. Macromolecules 1986;19:636–43.
[58] Kitamaru R, Nakaoki T, Alamo RG, Mandelkern L. Macromolecules 1996;29:6847–52.
[59] Kaji H, Horii F. Macromolecules 1997;30:5791–8.
[60] Van Amerongen GJ. J Polym Sci 1950;5:307–32.
[61] Paul DR, Di Benedetto AT. J Polym Sci Part C 1965;10:17–44.
[62] Durrill PL, Griskey RG. AIChE J 1966;12:1147–51.
[63] Durrill PL, Griskey RG. AIChE J 1969;15:106–10.